

# Effects of Chlorine Addition on Nitrogen Oxide Reduction and Mercury Oxidation over Selective Catalytic Reduction Catalysts

Mingxuan Ji, Honghu Li, Kang Hu, and Jiangjun Hu\*

Cite This: *ACS Omega* 2022, 7, 12098–12110

Read Online

ACCESS |



Metrics &amp; More

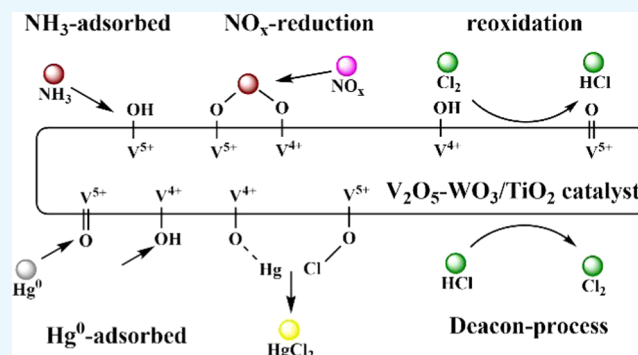


Article Recommendations



Supporting Information

**ABSTRACT:** The effect of chlorine on mercury oxidation and nitrogen oxides ( $\text{NO}_x$ ) reduction over selective catalytic reduction (SCR) catalysts was investigated in this study. Commercial SCR catalysts achieved a high  $\text{Hg}^0$  oxidation efficiency when  $\text{Cl}_2$  was sprayed into the flue gas. Results indicated that an appropriate concentration of  $\text{Cl}_2$  was found to promote  $\text{NO}_x$  reduction and  $\text{Hg}^0$  oxidation significantly. An optimal concentration of  $\text{Cl}_2$  (25 ppm) was found to significantly promote  $\text{NO}_x$  reduction and  $\text{Hg}^0$  oxidation. Moreover, we studied the effects of  $\text{Cl}_2$  on  $\text{NO}_x$  reduction and  $\text{Hg}^0$  oxidation over SCR catalysts under different concentrations of  $\text{SO}_2$ . The  $\text{SO}_2$  poisoning effect was decreased by  $\text{Cl}_2$  when the  $\text{SO}_2$  concentration was low (below 1500 ppm). However, sulfate gradually covered the catalyst surface over time during the reaction, which limited the impact of  $\text{Cl}_2$ . Finally, different sulfur-poisoned catalysts were examined in the presence of  $\text{Cl}_2$ . The  $\text{NO}_x$  reduction and  $\text{Hg}^0$  oxidation performances of sulfate-poisoned catalysts improved when  $\text{Cl}_2$  was added to the flue gas. Mechanisms for  $\text{NO}_x$  reduction and  $\text{Hg}^0$  oxidation over fresh catalysts and sulfate-poisoned catalysts in the presence of  $\text{Cl}_2$  were proposed in this study. The mechanism of  $\text{Cl}_2$ -influenced  $\text{NO}_x$  reduction was similar to that for the  $\text{NH}_3$ -SCR process. With  $\text{Cl}_2$  in the flue gas, the number of Brønsted active sites increased, which improved catalytic activity. Furthermore,  $\text{Cl}_2$  reoxidized  $\text{V}^{4+}\text{-OH}$  to  $\text{V}^{5+}=\text{O}$  and caused the  $\text{NH}_3$ -SCR process to operate continuously. The Langmuir–Hinshelwood mechanism was followed for  $\text{Hg}^0$  oxidation by SCR catalysts when  $\text{Cl}_2$  was in the flue gas.  $\text{Cl}_2$  increased the number of Lewis active sites, and catalytic activity increased.  $\text{Hg}^0$  adsorbed on the surface of the catalysts and was then oxidized to  $\text{HgCl}_2$ . Adding  $\text{Cl}_2$  to the flue gas increased the strength and number of acid sites on sulfate-poisoned catalysts.



## 1. INTRODUCTION

Mercury is highly toxic, volatile, persistent in the environment, and can bioaccumulate in living organisms.<sup>1,2</sup> Mercury pollution has significant impacts on human health; it leads to the loss of sensory or cognitive ability and can cause tremors, inability to walk, convulsions, and death.<sup>3</sup> Coal-fired power plants are the major anthropogenic source of mercury emissions into the atmosphere.<sup>4,5</sup> Once emitted into the atmosphere, elemental mercury can persist for weeks and travel long distances until it is oxidized, whereupon it can deposit in water bodies and enter the food chain.<sup>4</sup> Mercury exists in three forms in the flue gas produced by coal combustion: elemental ( $\text{Hg}^0$ ), oxidized ( $\text{Hg}^{2+}$ ), and particulate-bound species ( $\text{Hg}_p$ ). The oxidized mercury ( $\text{Hg}^{2+}$ ) and particle mercury ( $\text{Hg}_p$ ) can be easily removed using existing pollution control devices, such as in wet flue gas desulfurization and dedusting equipment, but  $\text{Hg}^0$  is difficult to capture because it is water-insoluble and has high volatility.<sup>6</sup>

The primary methods for capturing  $\text{Hg}^0$  are adsorbent- or oxidation-based methods.<sup>7</sup> Activated carbon and modified activated carbon are commonly used mercury-removal adsorbents due to their large specific surface areas, high

surface reactivities, and favorable pore sizes. Activated carbon adsorbs  $\text{Hg}^0$  on its surface and is usually injected upstream of a particulate control device in the removal process. However, the application of activated-carbon-based adsorbents is limited by the high cost of operation and the difficulty of reclaiming fly ash.<sup>7,8</sup> Oxidation-based removal methods convert  $\text{Hg}^0$  into  $\text{Hg}^{2+}$ . For example, Fenton and Fenton-like reagents were prepared by introducing  $\text{Fe}^{2+}$ ,  $\text{Cu}^{2+}$ , and  $\text{Mn}^{2+}$  into hydrogen peroxide. Additional  $\cdot\text{OH}$  ions were generated when the introduced metal ions increased  $\text{H}_2\text{O}_2$  decomposition, resulting in the oxidation of  $\text{Hg}^0$  to  $\text{Hg}^{2+}$ .<sup>7</sup> Acidic potassium permanganate solution, commonly used as an absorbent for the Ontario Hydro method, readily oxidizes  $\text{Hg}^0$ .<sup>9</sup> However, higher costs are incurred when capturing  $\text{Hg}^0$  with Fenton

Received: January 18, 2022

Accepted: March 15, 2022

Published: March 29, 2022



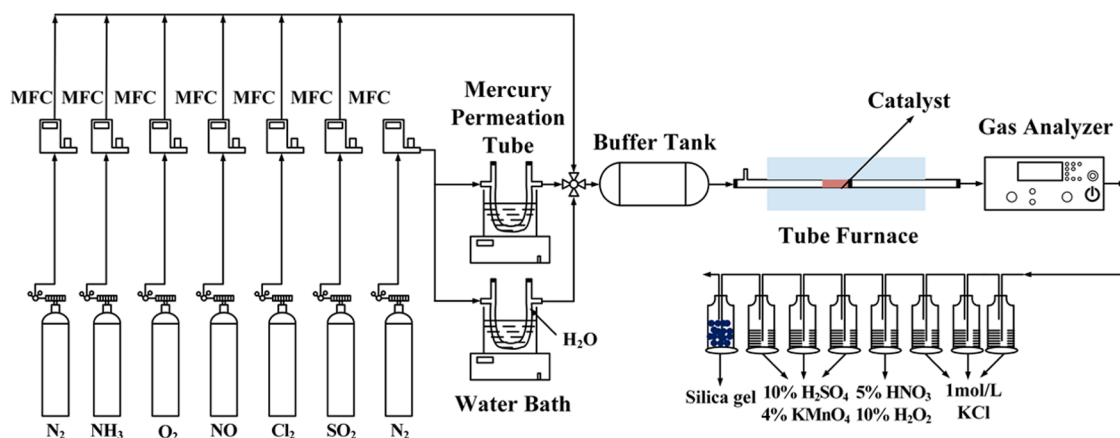


Figure 1. Schematic diagram of the experimental system.

reagent, Fenton-like reagent, or acidic potassium permanganate solution.

One cost-effective process for oxidizing and removing  $\text{Hg}^0$  is selective catalytic reduction (SCR).<sup>10</sup> Coal-fired power plants widely use the SCR method for  $\text{NO}_x$  reduction.  $\text{NH}_3$  reduces  $\text{NO}_x$  in the flue gas over the surface of an SCR catalyst to produce  $\text{N}_2$  and  $\text{H}_2\text{O}$ ;  $\text{Hg}^0$  is oxidized to  $\text{Hg}^{2+}$  when the flue gas passes through the SCR catalyst. However,  $\text{Hg}^0$  oxidation using commercial SCR catalysts ( $\text{V}_2\text{O}_5$ - $\text{WO}_3$ / $\text{TiO}_2$ ) typically exhibits a low efficiency.<sup>11</sup> Therefore, two methods were proposed in previous studies to increase the efficiency of  $\text{Hg}^0$  oxidation in flue gas: (1) synthesis of effective transition-metal-oxide catalysts, such as Mn-based catalysts,<sup>12</sup> Cu-based catalysts,<sup>13</sup> or Co-based catalysts;<sup>14</sup> (2) addition of halogen compounds such as hydrogen chloride (HCl) or chlorine ( $\text{Cl}_2$ ) into coal-fired power plant flue gas.<sup>15,16</sup> Previous studies have investigated the effect of HCl on  $\text{Hg}^0$  oxidation over SCR catalysts, but there is limited research on the effect of  $\text{Cl}_2$  addition on this process.<sup>11,17</sup> Furthermore, there has not been sufficient research on the effects of  $\text{Cl}_2$  addition on simultaneous  $\text{NO}_x$  conversion and  $\text{Hg}^0$  oxidation over SCR catalysts.

We designed three sets of experiments in this study. In set 1,  $\text{Cl}_2$  was added to flue gas in various concentrations to investigate the effects on  $\text{NO}_x$  conversion and  $\text{Hg}^0$  oxidation over the surface of fresh SCR catalysts. The mechanism of how  $\text{Cl}_2$  impacts  $\text{NO}_x$  reduction and  $\text{Hg}^0$  oxidation is discussed below. In set 2, we added different concentrations of  $\text{SO}_2$  to flue gas, and the effects of  $\text{Cl}_2$  on  $\text{NO}_x$  conversion and  $\text{Hg}^0$  oxidation over fresh catalysts under these conditions were investigated. Finally, in set 3, we studied the effects of chlorine addition on  $\text{NO}_x$  conversion and  $\text{Hg}^0$  oxidation over different sulfur-poisoned catalysts. A proposed mechanism for the influence of  $\text{Cl}_2$  on  $\text{NO}_x$  reduction and  $\text{Hg}^0$  oxidation over different sulfur-poisoned catalysts was also described.

## 2. MATERIALS AND METHODS

**2.1. Catalyst Preparation.** The fresh SCR catalysts used in this study are honeycomb commercial catalysts purchased from Yigang Environmental Engineering Materials Co. Ltd., China. The honeycomb catalysts were first ground to powder and then sieved with a sifter. A powder with a particle size of <60 mesh was used in the experiments as a fresh catalyst.

The SCR catalysts poisoned by sulfate were synthesized using the fresh SCR catalysts. Fresh SCR catalysts were

immersed in different sulfate solutions including 0, 0.1, 0.3, and 0.5 mol/L  $\text{NH}_4\text{HSO}_4$  solution, 0.1 mol/L  $\text{CaSO}_4$  solution, and 0.1 mol/L  $\text{MgSO}_4$  solution. First, 5 g of fresh SCR catalyst was poured into 300 mL of each sulfate solution and stirred for 4 h. Then, each sulfate solution was filtered and the precipitate was dried in a desiccator for 24 h. Next, the precipitates were ground to powder and sieved with a sifter. A powder with a particle size of <60 mesh was used in the experiments as a sulfate-poisoned catalyst.

**2.2. Catalyst Evaluation.** The catalytic activity for  $\text{NO}_x$  conversion and  $\text{Hg}^0$  oxidation was carried out in a fixed-bed flow reactor. The schematic diagram of the experimental setup is shown in Figure 1. The experimental apparatus contained four parts: a simulation flow gas generating system, a fixed-bed reactor, a flue gas test system, and a mercury gas test system.

The simulation flow gas generating system included a gas-component-generating device and a mercury-vapor-generating device. The components of the flue gas were from cylinder gases and were precisely controlled by mass flow controllers, with a total gas flow rate of 1000 mL/min. Mercury vapor from a mercury permeation tube (HE-SR, VICI Metronics) placed in a water bath was the source of elemental mercury. The concentration of  $\text{Hg}^0$  was approximately  $65 \mu\text{g}/\text{m}^3$ .<sup>3,18</sup> Before entering the reactor, mercury vapor was carried by  $\text{N}_2$  and mixed thoroughly with other gases in a buffer tank.

The fixed-bed reactor included a quartz tube and a tubular electric furnace. The quartz tube with an inner diameter of 10 mm and a length of 1000 mm was loaded with 0.5 g of catalyst, with the aid of quartz wool to keep the catalyst fixed in the quartz tube. The quartz tube was placed in a tubular electric furnace to maintain the reaction temperature. The  $\text{NO}_x$  conversion and mercury oxidation reactions were performed at a temperature of 350 °C, which was the optimal temperature for the catalysts.

The  $\text{NO}_x$  concentrations in the inlet and outlet gas were measured by a gas analyzer (Ecom-J2KN, Germany). The mercury in the simulated gas was sampled simultaneously using the Ontario Hydro method (OHM).<sup>9</sup>  $\text{Hg}^{2+}$  was absorbed in the 1 mol/L KCl solution,  $\text{Hg}^0$  was absorbed in the 5%  $\text{HNO}_3$ -10%  $\text{H}_2\text{O}_2$  and 4%  $\text{KMnO}_4$ -10%  $\text{H}_2\text{SO}_4$  solution. The concentrations of  $\text{Hg}^{2+}$  and  $\text{Hg}^0$  in the absorbent solution were detected by inductively coupled plasma mass spectrometry (PQ-MS, Analytik Jena AG, Germany) after recovery and digestion.

In each test, it took at least 30 min to obtain steady  $\text{Hg}_{\text{in}}^0$  and  $\text{NO}_{x_{\text{in}}}$  concentrations. Saturated  $\text{Hg}^0$  was adsorbed on the catalysts. The test data were recorded after 60 min of reaction. The  $\text{NO}_x$  conversion and  $\text{Hg}^0$  oxidation efficiency were calculated using eqs 1 and 2

$$\eta_{\text{NO}_x} = \frac{\text{NO}_{x_{\text{in}}} - \text{NO}_{x_{\text{out}}}}{\text{NO}_{x_{\text{in}}}} \times 100\% \quad (1)$$

$$\eta_{\text{Hg}^0} = \frac{\text{Hg}_{\text{in}}^0 - \text{Hg}_{\text{out}}^0}{\text{Hg}_{\text{in}}^0} \times 100\% \quad (2)$$

The three sets of experiments designed in this study are summarized in Table 1. Set 1 was conducted to confirm that

**Table 1. Design of Three Sets of Experiments**

set	catalysts	gas components	
		$\text{SO}_2$ (ppm)	$\text{Cl}_2$ (ppm)
Set 1	SCR	500	0–30
Set 2	SCR	0–2500	25
Set 2	SCR	0–2500	0
Set 3	$\text{NH}_4\text{HSO}_4$ -SCR	500	25
Set 3	$\text{NH}_4\text{HSO}_4$ -SCR	500	0
Set 3	$\text{CaSO}_4$ -SCR	500	25
Set 3	$\text{CaSO}_4$ -SCR	500	0
Set 3	$\text{MgSO}_4$ -SCR	500	25
Set 3	$\text{MgSO}_4$ -SCR	500	0

$\text{Cl}_2$  can improve  $\text{NO}_x$  reduction and  $\text{Hg}^0$  oxidation efficiency over SCR catalysts and to determine the optimal  $\text{Cl}_2$  concentration for enhanced  $\text{NO}_x$  reduction and  $\text{Hg}^0$  oxidation. Set 2 was conducted to show that  $\text{Cl}_2$  can improve  $\text{NO}_x$  reduction and  $\text{Hg}^0$  oxidation under different  $\text{SO}_2$  concentrations. Set 3 was conducted to show that  $\text{Cl}_2$  can improve  $\text{NO}_x$  reduction and  $\text{Hg}^0$  oxidation over different sulfur-poisoned catalysts.

All experiments mentioned in the table were carried out at 350 °C. The space velocity of the experiments was  $3 \times 10^4 \text{ h}^{-1}$ . The concentration of  $\text{Hg}^0$  was approximately  $65 \mu\text{g}/\text{m}^3$ .<sup>18</sup> The concentrations of  $\text{NO}$  and  $\text{NH}_3$  were 500 ppm, and the concentrations of  $\text{O}_2$  and  $\text{H}_2\text{O}$  were 5%. The concentration units of  $\text{NO}$ ,  $\text{NH}_3$ ,  $\text{SO}_2$ , and  $\text{Cl}_2$  were ppm, and the concentrations of  $\text{O}_2$  and  $\text{H}_2\text{O}$  were volume fractions of the total gas flow.

**2.3. Catalyst Characterization.** The chemical components of the catalysts were determined using an X-ray fluorescence spectrometer (XRF). The specific surface area and pore volume were determined using the Brunauer–Emmett–Teller (BET) method. X-ray diffraction (XRD) and transmission electron microscopy (TEM) were used to examine the microstructure of the catalysts. X-ray photoelectron spectroscopy (XPS) and Fourier transform infrared (FTIR) spectroscopy were used to analyze the reactions of the SCR process. Temperature-programmed reduction ( $\text{H}_2$ -TPR) was used to find the most efficient reduction conditions of the catalysts. Temperature-programmed desorption of ammonia ( $\text{NH}_3$ -TPD) was used to analyze the active sites on the catalysts. The instruments and detailed instructions are described as follows:

(1) XRF was performed using an ARL PERFORM'X sequential X-ray fluorescence spectrometer, and the

results were used to determine the chemical components of the catalysts.

- (2) BET: The specific surface area and pore volume were determined by  $\text{N}_2$  adsorption isotherms at 77 K using a Micromeritics ASAP 2460 analyzer.
- (3) XRD patterns of the catalysts were carried out using a diffractometer and obtained in the  $2\theta$  range from 10 to 80 with  $\text{Cu K}\alpha$  radiation ( $\lambda = 1.54 \text{ \AA}$ ).
- (4) TEM was performed using a JEOL JEM-2100 instrument and was used to examine the morphology of the SCR catalysts.
- (5) XPS experiments were performed using an ESCALAB 250Xi high-performance electron spectrometer, using  $\text{Al K}\alpha$  (1486.6 eV) as the excitation source (12.5 kV, 16 mA). The sample charging effects were compensated for by calibrating all binding energies (BEs) with the adventitious C 1s peak at 284.8 eV.
- (6) FTIR spectroscopy was conducted using an FTIR 5700 to analyze the chemical functional groups on the SCR catalyst surface. The SCR catalyst sample powders were mixed with potassium bromide (KBr), ground, and pressed into self-supporting disks. The ratio of the weight of the SCR catalyst sample to that of KBr was 1:100. The skeletal spectra ranged from 4000 to 400  $\text{cm}^{-1}$  with a resolution of 4  $\text{cm}^{-1}$ .
- (7)  $\text{H}_2$ -TPR experiments were performed using an AUTO CHEM 2920. Prior to the  $\text{H}_2$ -TPR test, 100 mg of sample was heated from room temperature to 300 °C in He gas flow at the rate of 10 °C/min for pretreatment and purged at 300 °C for 1 h in He gas flow, then cooled to 50 °C.  $\text{H}_2$  adsorption was carried out at 50 °C using a 10%  $\text{H}_2/\text{He}$  gas mixture (30–50 mL/min) until saturation of the sample. Then, the sample was exposed to a flow of He (30 mL/h) to remove the weakly absorbed  $\text{H}_2$  at 50 °C. Finally, the catalyst was heated from 50 to 800 °C in He gas flow at the rate of 10 °C/min; the outlet gas was detected with TCD.
- (8)  $\text{NH}_3$ -TPD experiments were performed using an AUTO CHEM 2920. Prior to the  $\text{NH}_3$ -TPD test, 100 mg of sample was heated from room temperature to 300 °C in He gas flow at the rate of 10 °C/min for pretreatment and purged at 300 °C for 1 h in He gas flow, then cooled to 50 °C.  $\text{NH}_3$  adsorption was carried out at 50 °C using a 10%  $\text{NH}_3/\text{He}$  gas mixture (30–50 mL/min) until saturation of the sample. Then, the sample was exposed to a flow of He (30 mL/h) to remove the weakly absorbed  $\text{NH}_3$  at 50 °C. Finally, the catalyst was heated from 50 to 800 °C in He gas flow at the rate of 10 °C/min and the outlet gas was detected with TCD.

### 3. RESULTS AND DISCUSSION

**3.1. Effect of  $\text{Cl}_2$  Addition on  $\text{NO}_x$  Reduction and  $\text{Hg}^0$  Oxidation by Fresh Catalysts.**  $\text{Cl}_2$  is known to influence  $\text{NO}_x$  reduction and  $\text{Hg}^0$  oxidation over SCR catalysts;<sup>11,19</sup> thus, it is necessary to investigate these effects. The conditions of the experiments are listed in Table 1 Set 1.

**3.1.1. Effect of  $\text{Cl}_2$  on  $\text{NO}_x$  Conversion over Fresh Catalysts.** The SCR process is typically used to reduce  $\text{NO}_x$  in flue gas.<sup>20</sup>  $\text{Cl}_2$  sprayed into the flue gas may affect  $\text{NO}_x$  reduction over SCR catalysts. In this study, the impact of  $\text{Cl}_2$  on  $\text{NO}_x$  reduction over SCR catalysts was studied for a series of  $\text{Cl}_2$  concentrations. As displayed in Figure 2a, the  $\text{NO}_x$

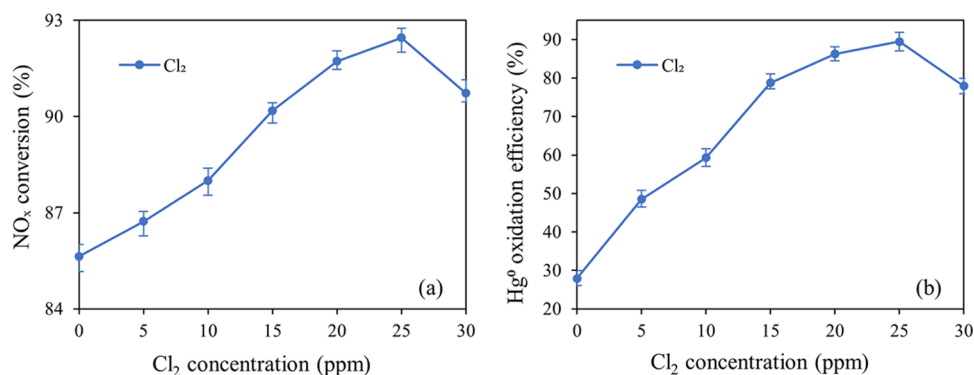


**Figure 2.** Effect of different concentrations of  $\text{Cl}_2$  on (a)  $\text{NO}_x$  conversion and (b)  $\text{Hg}^0$  oxidation efficiency over SCR catalysts.

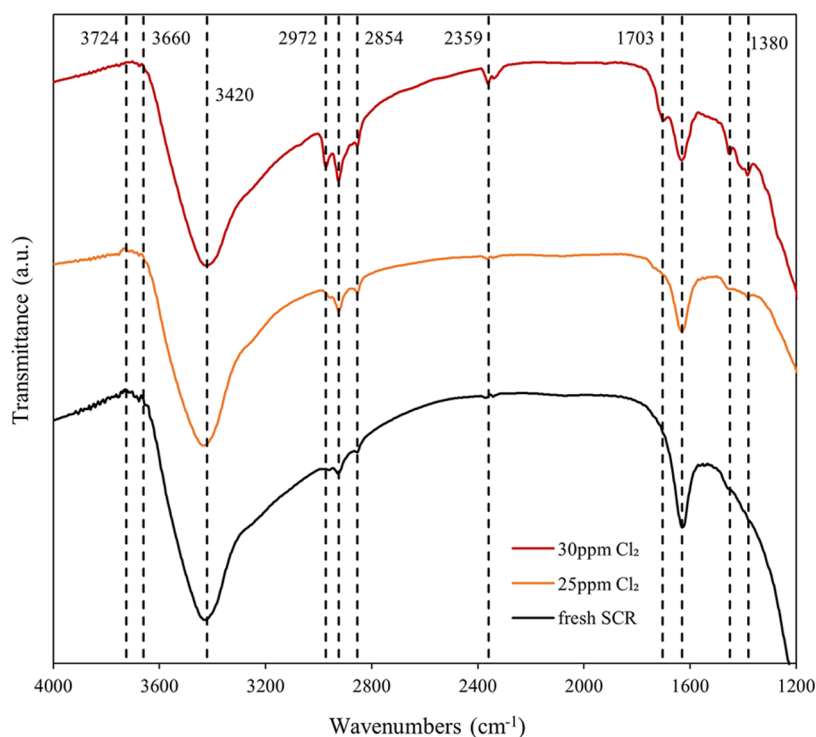


**Figure 3.** Infrared spectra under different conditions in the region of  $4000\text{--}1200\text{ cm}^{-1}$ .

conversion rate was approximately 86% on SCR catalysts in the absence of  $\text{Cl}_2$ . The Eley–Rideal mechanism, wherein  $\text{NH}_3$  is adsorbed on the catalysts and reacts with  $\text{NO}_x$  in the gas phase, describes  $\text{NO}_x$  reduction on SCR catalysts.  $\text{O}_2$  plays a substantial role in the SCR process;<sup>21</sup> it oxidizes the active sites on the catalyst surface and keeps the SCR process operating continuously. When 5 and 10 ppm of  $\text{Cl}_2$  were added to the gas, the  $\text{NO}_x$  conversion efficiency increased slightly. When the  $\text{Cl}_2$  content was further increased from 15 to 25 ppm, the efficiency increased from 90% to approximately 93%. At higher temperatures,  $\text{Cl}_2$  becomes an even stronger oxidizing agent.<sup>22,23</sup> In addition to  $\text{O}_2$ ,  $\text{Cl}_2$  can oxidize the active sites on the SCR catalysts and ensure that the process continues. In other words,  $\text{Cl}_2$  plays the same role as that of oxygen in the reaction and improves the  $\text{NO}_x$  reduction reaction efficiency at  $350\text{ }^\circ\text{C}$ . However, when the  $\text{Cl}_2$  content increased to 30 ppm,  $\text{NO}_x$  reduction reaction efficiency decreased slightly. This may correspond to poor catalyst redox properties and a decrease in the number of active sites on the catalyst surface.

**3.1.2. Effect of  $\text{Cl}_2$  on  $\text{Hg}^0$  Oxidation over Fresh Catalysts.** Gas-phase  $\text{Hg}^0$  can react with several gas-phase  $\text{Cl}_2$  compounds, such as  $\text{Cl}_2$ ,<sup>15,16</sup>  $\text{HCl}$ ,<sup>15</sup> and chlorine radicals.<sup>24</sup> Although the homogeneous reaction between  $\text{Hg}^0$  and  $\text{Cl}_2$  is too slow to cause significant  $\text{Hg}^0$  conversion,  $\text{Cl}_2$  can promote  $\text{Hg}^0$  oxidation efficiency over SCR catalysts.<sup>25</sup> The impact of  $\text{Cl}_2$  on  $\text{Hg}^0$  removal was studied over a series of  $\text{Cl}_2$  concentrations. As presented in Figure 2b, only approximately 28% of the  $\text{Hg}^0$  was oxidized over SCR catalysts in the absence of  $\text{Cl}_2$ . When the flue gas contained only 5%  $\text{O}_2$  without other  $\text{Cl}_2$  compounds, the  $\text{Hg}^0$  oxidation efficiency was very low.<sup>11,26</sup> Thus, it is necessary to add some  $\text{Cl}_2$  compounds to improve the oxidation rate. The SCR catalysts first showed an increasing trend and then a decreasing trend in  $\text{Hg}^0$  oxidation efficiency as the  $\text{Cl}_2$  concentration increased from 5 to 30 ppm. As the  $\text{Cl}_2$  concentration increased from 5 to 25 ppm, the  $\text{Hg}^0$  oxidation efficiency increased from 48 to 89%. These results suggest that  $\text{Cl}_2$  in flue gas can promote the  $\text{Hg}^0$  oxidation process.<sup>27</sup> As the  $\text{Cl}_2$  concentration increased from 25 to 30 ppm, the  $\text{Hg}^0$  oxidation efficiency decreased to 78%. At the

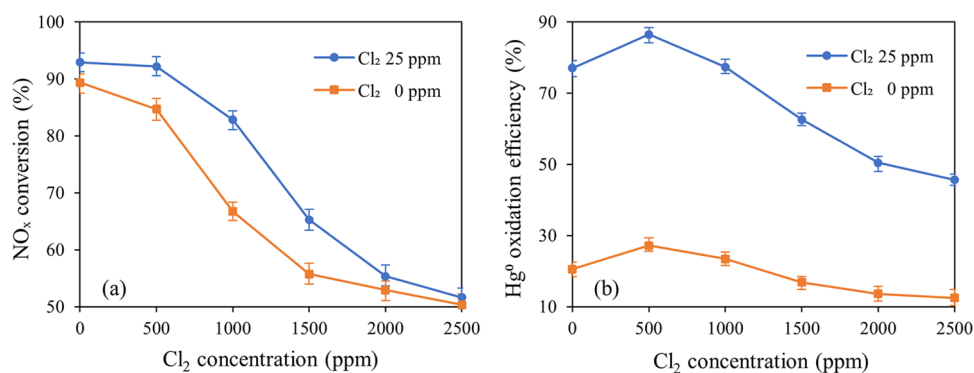
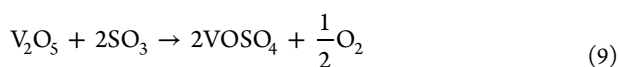
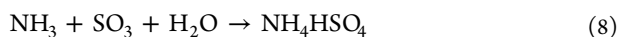
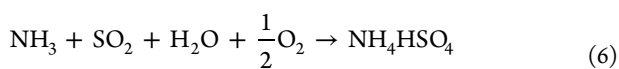
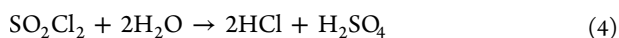
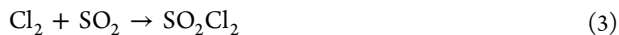


**Figure 4.** Effect of different concentrations of SO<sub>2</sub> on (a) NO<sub>x</sub> conversion and (b) Hg<sup>0</sup> oxidation efficiency over SCR catalysts in the presence of Cl<sub>2</sub>.

highest concentrations of Cl<sub>2</sub>, SO<sub>2</sub> may be oxidizing into high-valency sulfur compounds, such as sulfuryl chloride (SO<sub>2</sub>Cl<sub>2</sub>), sulfur trioxide (SO<sub>3</sub>), or sulfuric acid (H<sub>2</sub>SO<sub>4</sub>) (eqs 3–5), which react with ammonia and vanadium pentoxide to generate ammonium sulfates<sup>28</sup> or vanadyl sulfate (VOSO<sub>4</sub>)<sup>29</sup> (eqs 6–10). Figure 3 displays the FTIR spectra of the catalysts. The bands at 3724 and 3660 cm<sup>-1</sup> can be attributed to the hydroxyl groups on TiO<sub>2</sub>.<sup>30,31</sup> Infrared spectra of VOSO<sub>4</sub> showed two broad bands at 1630 and 1410 cm<sup>-1</sup> and S=O shows a band at 1410 cm<sup>-1</sup>.<sup>30,32,33</sup> The bands at 1450 and 1703 cm<sup>-1</sup> were assigned to the asymmetric bending vibration of NH<sub>4</sub><sup>+</sup> and symmetric bending of NH<sub>4</sub><sup>+</sup>, respectively. The bands from 3000 to 2600 cm<sup>-1</sup> caused by protonated ammonia species were also observed (2972, 2924, and 2854 cm<sup>-1</sup>).<sup>30,34,35</sup> The FTIR spectra of the catalysts showed that (NH<sub>4</sub>)<sub>2</sub>SO<sub>4</sub> and VOSO<sub>4</sub> were generated on the catalysts, forming metal sulfates and ammonium sulfates that occupied the active sites on the surface of the catalysts and gradually deactivated the catalysts throughout the reaction. Thus, 30 ppm Cl<sub>2</sub> reduced the Hg<sup>0</sup> oxidation efficiency.

As discussed in Sections 3.1.1 and 3.1.2, 30 ppm Cl<sub>2</sub> reduced the NO<sub>x</sub> reduction reaction efficiency and the Hg<sup>0</sup> oxidation rate. Hence, 25 ppm Cl<sub>2</sub> was considered optimal and was used in the experiments.



### 3.2. Effect of SO<sub>2</sub> on NO<sub>x</sub> Reduction and Hg<sup>0</sup> Oxidation over Fresh Catalysts in the Presence of Cl<sub>2</sub>.

SO<sub>2</sub> is known to poison SCR catalysts, destroy the catalyst structures, and reduce the catalyst activities. Thus, the influence of SO<sub>2</sub> on the performance of fresh catalysts for NO<sub>x</sub> conversion and Hg<sup>0</sup> oxidation efficiency requires further research. The conditions of the experiments are listed in Table 1 Set 2. One set of experiments labeled the test group was operated at 25 ppm Cl<sub>2</sub>, while the other set of experiments was run at 0 ppm Cl<sub>2</sub> as a control.

**3.2.1. Effect of SO<sub>2</sub> on NO<sub>x</sub> Conversion in the Presence of Cl<sub>2</sub>.** The activity of SCR catalysts decreased in the presence of SO<sub>2</sub> in the flue gas, but the presence of Cl<sub>2</sub> diminished the degree of SO<sub>2</sub> influence. As shown in Figure 4a, as the SO<sub>2</sub> concentration increased from 0 to 2500 ppm, the NO<sub>x</sub> conversion efficiency decreased with and without Cl<sub>2</sub>. Therefore, the existence of SO<sub>2</sub> in the flue gas reduces the NO<sub>x</sub> conversion efficiency. However, at 500 ppm SO<sub>2</sub> and 25 ppm Cl<sub>2</sub>, the NO<sub>x</sub> conversion efficiency was approximately 92%, which was approximately 8% higher than that without Cl<sub>2</sub>. At 1000 ppm SO<sub>2</sub> and 25 ppm Cl<sub>2</sub>, the NO<sub>x</sub> conversion efficiency was approximately 82%, which was approximately 16% higher than that without Cl<sub>2</sub>. When the SO<sub>2</sub> concentration increased to 1500 ppm, the results were similar, but when it was increased to 2000 or 2500 ppm, the NO<sub>x</sub> conversion efficiency was approximately the same with or without Cl<sub>2</sub>. For SO<sub>2</sub> concentrations below 1500 ppm, Cl<sub>2</sub> diminished the effect of SO<sub>2</sub> on NO<sub>x</sub> conversion efficiency, whereas for SO<sub>2</sub> concentrations above 1500 ppm, the NO<sub>x</sub> conversion efficiency showed no difference.

**3.2.2. Effect of SO<sub>2</sub> on Hg<sup>0</sup> Oxidation in the Presence of Cl<sub>2</sub>.** As shown in Figure 4b, as the concentration of SO<sub>2</sub> increased from 0 to 2500 ppm, Hg<sup>0</sup> oxidation efficiency first increased and then decreased both in the presence and absence of Cl<sub>2</sub> in the flue gas. When SO<sub>2</sub> concentrations increased to 500 ppm, the Hg<sup>0</sup> oxidation efficiency reached the maximum value. With the aid of O<sub>2</sub>, low concentrations of SO<sub>2</sub> promoted Hg<sup>0</sup> oxidation, while high concentrations of SO<sub>2</sub> deteriorated Hg<sup>0</sup> oxidation.<sup>36,37</sup> Metal-oxide-based SCR catalysts are known to oxidize SO<sub>2</sub> to form SO<sub>3</sub>.<sup>38,39</sup> During the Hg<sup>0</sup> oxidation process, SO<sub>3</sub> facilitates Hg<sup>0</sup> oxidation and mercury sulfate (HgSO<sub>4</sub>) forms (eqs 11–13). As SO<sub>2</sub> concentrations increase to higher levels, the inhibitive influence of SO<sub>2</sub> prevails over its promotional effect over SCR catalysts.<sup>37</sup> Sulfur oxides (SO<sub>x</sub>) react with ammonia, generating ammonium sulfate or ammonium bisulfate, which occupies the activity sites of SCR catalysts,<sup>28,40</sup> or reacts with vanadium oxide, generating

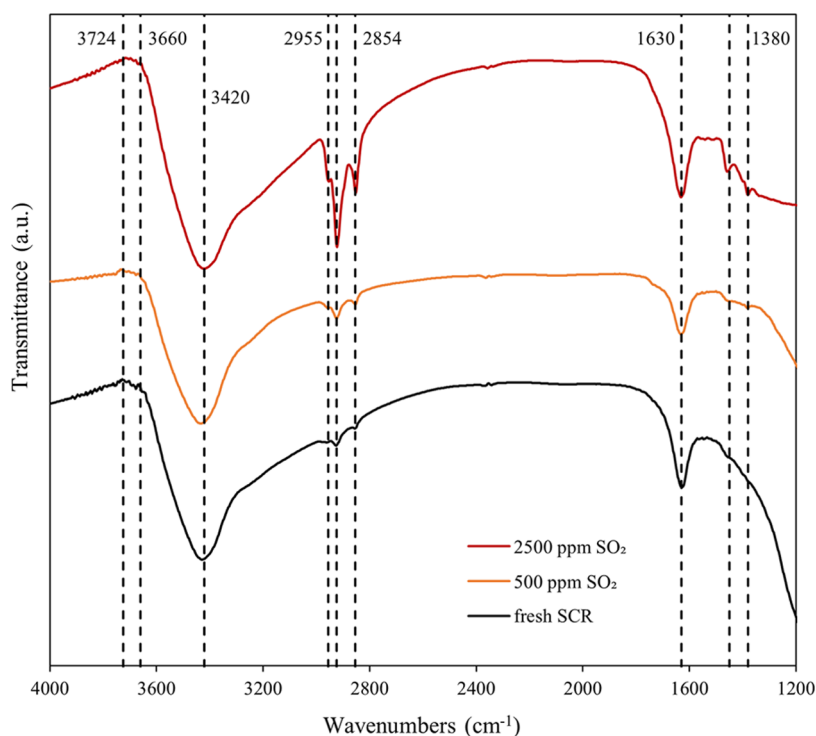


Figure 5. Infrared spectra of different conditions in the region of 4000–1200  $\text{cm}^{-1}$ .

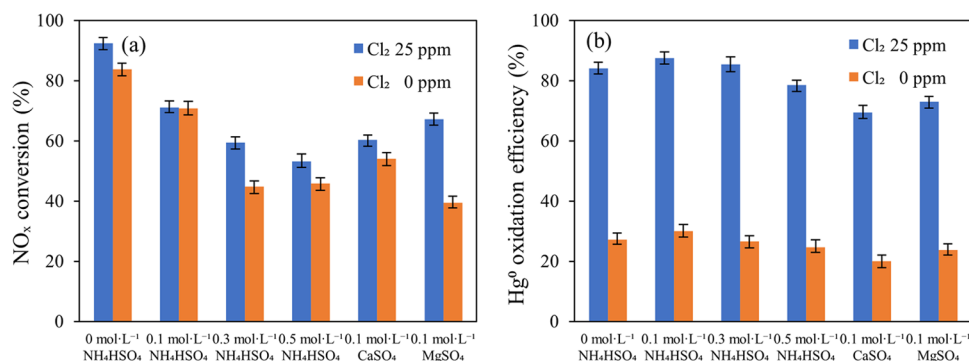


Figure 6. Effect of  $\text{Cl}_2$  on (a)  $\text{NO}_x$  conversion and (b)  $\text{Hg}^0$  oxidation efficiency over different sulfate-poisoned catalysts.

vanadyl sulfate ( $\text{VOSO}_4$ ), which destroys the structure of the catalysts.<sup>29</sup> Thus, low  $\text{SO}_2$  concentrations facilitate  $\text{Hg}^0$  oxidation, but high concentrations lead to its inhibition. Figure 5 displays the FTIR spectra of the catalysts. The bands at 3724 and 3660  $\text{cm}^{-1}$  can be attributed to the hydroxyl groups on  $\text{TiO}_2$ .<sup>30,31</sup> The FTIR spectra of  $\text{VOSO}_4$  shows two broad bands at 1630 and 1380  $\text{cm}^{-1}$  and  $\text{S}=\text{O}$  shows a band at 1410  $\text{cm}^{-1}$ .<sup>30,32,33</sup> The bands around 3000–2600  $\text{cm}^{-1}$  caused by protonated ammonia species were also observed (2955, 2924, and 2854  $\text{cm}^{-1}$ ).<sup>30,34,35</sup> The FTIR spectra of the catalysts illustrated that  $(\text{NH}_4)_2\text{SO}_4$  and  $\text{VOSO}_4$  were generated on the catalysts. This formed metal sulfates and ammonium sulfates that occupied the active sites on the surface of the catalysts and gradually deactivated the catalysts throughout the reaction.

The addition of  $\text{Cl}_2$  to the flue gas diminished the effect of  $\text{SO}_2$  on  $\text{Hg}^0$  catalytic oxidation.<sup>36,41</sup> As shown in Figure 4b, as the concentration of  $\text{SO}_2$  ranged from 0 to 2500 ppm, the  $\text{Hg}^0$  oxidation efficiency in the presence of  $\text{Cl}_2$  was much higher than that in the absence of  $\text{Cl}_2$ . The results showed that  $\text{Cl}_2$  and  $\text{SO}_2$  exhibited competition for the activity sites on the

catalysts, and the addition of  $\text{Cl}_2$  into the flue gas prevented  $\text{SO}_2$  from occupying the activity sites.<sup>41</sup>  $\text{Cl}_2$  was activated over the activity sites and reacted with  $\text{Hg}^0$  preferentially. Therefore,  $\text{Cl}_2$  diminished the effect of  $\text{SO}_2$  on  $\text{Hg}^0$  catalytic oxidation.

### 3.3. Effect of $\text{Cl}_2$ on $\text{NO}_x$ Reduction and $\text{Hg}^0$ Oxidation over Sulfate-Poisoned Catalysts.

After extended operating times, different types of sulfates may cover the surface of the SCR catalysts. According to the results of the experiments described in Sections 3.1.1 and 3.1.2,  $\text{Cl}_2$  is known to improve the performance of the poisoned catalysts for  $\text{NO}_x$  reduction and  $\text{Hg}^0$  oxidation. Therefore, it is necessary to thoroughly investigate the effect of  $\text{Cl}_2$  addition on  $\text{NO}_x$  conversion and  $\text{Hg}^0$  oxidation by sulfate-poisoned catalysts. The preparation of sulfate-poisoned catalysts is presented in Section 2.1, and the experimental conditions are listed in Table 1 Set 3. Note that the 0 mol/L  $\text{NH}_4\text{HSO}_4$  experiment was the control group.

**3.3.1. Effect of  $\text{Cl}_2$  Addition on  $\text{NO}_x$  Conversion by Sulfate-Poisoned Catalysts.** Figure 6a presents the  $\text{NO}_x$  conversion efficiency over different sulfate-poisoned catalysts in the presence and absence of  $\text{Cl}_2$ . Different types of sulfates

inhibited the  $\text{NO}_x$  conversion efficiency by different amounts. As the concentration of  $\text{NH}_4\text{HSO}_4$  increased, the inhibitory influence increased significantly. The  $\text{NO}_x$  conversion efficiency of 0.5 mol/L  $\text{NH}_4\text{HSO}_4$  poisoned catalysts was lower than 50%. Previous studies showed that NO can be reduced by ammonia over  $\text{CaSO}_4$ ,<sup>42,43</sup> which decreases the inhibitory effect on  $\text{NO}_x$  conversion efficiency. When  $\text{Cl}_2$  was added to the flue gas, the  $\text{NO}_x$  reduction ability of sulfate-poisoned catalysts improved. The increase in efficiency was more than 10% over 0.3 and 0.5 mol/L  $\text{NH}_4\text{HSO}_4$ -poisoned catalysts. The  $\text{NO}_x$  conversion efficiency over  $\text{MgSO}_4$ -poisoned catalysts likewise showed a substantial increase of more than 10%. These results suggest that  $\text{Cl}_2$  can improve  $\text{NO}_x$  conversion efficiency over different sulfate-poisoned catalysts.

**3.3.2. Effect of  $\text{Cl}_2$  on  $\text{Hg}^0$  Oxidation over Sulfate-Poisoned Catalysts.** According to the results of the experiment in Section 3.2.2, the addition of  $\text{Cl}_2$  to flue gas increases the  $\text{Hg}^0$  oxidation rate. As shown in Figure 6b, the  $\text{Hg}^0$  oxidation efficiency is lower than 30% in the absence of  $\text{Cl}_2$ . The effects of different sulfate-poisoned catalysts on  $\text{Hg}^0$  oxidation were not evident because SCR catalysts have a weaker ability to oxidize  $\text{Hg}^0$  when no  $\text{Cl}_2$  exists in the flue gas.<sup>11</sup> When  $\text{Cl}_2$  was added to the flue gas,  $\text{Hg}^0$  oxidation efficiency increased to over 75%. Although sulfates had a slight inhibitory effect on the catalysts,  $\text{Cl}_2$  significantly promoted the  $\text{Hg}^0$  oxidation efficiency.

**3.4. Mechanisms of  $\text{Cl}_2$  Affecting  $\text{NO}_x$  Reduction and  $\text{Hg}^0$  Oxidation by  $\text{V}_2\text{O}_5\text{-WO}_3/\text{TiO}_2$  Catalysts.** **3.4.1. Mechanisms of  $\text{Cl}_2$  Affecting  $\text{NO}_x$  Reduction.** The reduction behavior of the active components in the catalysts was studied using  $\text{H}_2$ -TPR. For the  $\text{H}_2$ -TPR profile under 0 ppm  $\text{Cl}_2$  (Figure 7, profile (a)), there are two reduction peaks at

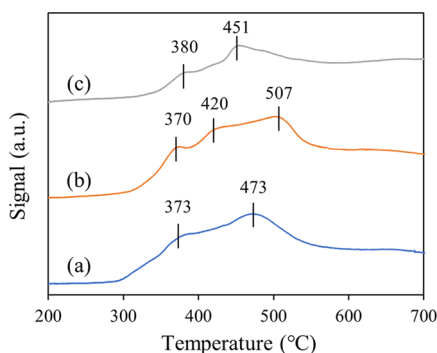


**Figure 7.**  $\text{H}_2$ -TPR profiles of catalysts exposed to different  $\text{Cl}_2$  concentrations. Flue gas conditions: 500 ppm  $\text{NO}$ , 500 ppm  $\text{NH}_3$ , 500 ppm  $\text{SO}_2$ , and 5%  $\text{O}_2$ ; (a) 0 ppm  $\text{Cl}_2$ , (b) 25 ppm  $\text{Cl}_2$ , and (c) 30 ppm  $\text{Cl}_2$ .

approximately 373 and 473 °C, which were ascribed to the reduction of  $\text{V}^{5+}$  to  $\text{V}^{3+}$  by highly dispersed, polymeric, vanadium species.<sup>44</sup> Monomeric vanadium species are reduced at a lower temperature than polymeric vanadium species, as previously reported.<sup>44,45</sup> Thus, the reduction peaks below 400 °C correspond to monomeric vanadium species, while the peaks at approximately 400–500 °C correspond to polymeric vanadium species. The profile under 25 ppm  $\text{Cl}_2$  (b) had an additional reduction peak at approximately from 300 to 500 °C, which was ascribed to the reduction of  $\text{V}^{5+}$  to  $\text{V}^{4+}$ .<sup>46</sup> The reduction peaks of polymeric vanadium shifted to higher values, indicating that more polymeric vanadium species might

have been formed. The two peaks of the profile under 30 ppm  $\text{Cl}_2$  (c) were much weaker, suggesting that the sample exhibited poor redox characteristics after exposure to this level of  $\text{Cl}_2$ .

Figure 8 contains the  $\text{H}_2$ -TPR profiles of samples after exposure to different concentrations of  $\text{SO}_2$ . The profile under

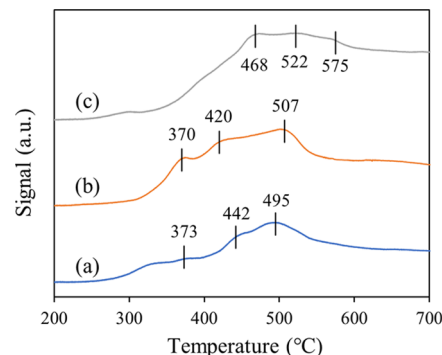


**Figure 8.**  $\text{H}_2$ -TPR profiles of catalysts exposed to different  $\text{SO}_2$  concentrations. Flue gas conditions: 500 ppm  $\text{NO}$ , 500 ppm  $\text{NH}_3$ , 25 ppm  $\text{Cl}_2$ , and 5%  $\text{O}_2$ ; (a) 0 ppm  $\text{SO}_2$ , (b) 500 ppm  $\text{SO}_2$ , and (c) 2500 ppm  $\text{SO}_2$ .

0 ppm  $\text{SO}_2$  (a) and the profile under 500 ppm  $\text{SO}_2$  (b) have three peaks corresponding to the reductions  $\text{V}_2\text{O}_5 \rightarrow \text{V}_2\text{O}_4 \rightarrow \text{V}_2\text{O}_3$ .<sup>47</sup> However, the reduction peaks of the profile under 2500 ppm  $\text{SO}_2$  (c) shifted to higher values. It was concluded that high concentrations of  $\text{SO}_2$  and the sulfate formed on the catalyst surface inhibited the reduction of vanadium.

The number and strengths of the acid sites in the SCR catalysts after exposure to different concentrations of  $\text{Cl}_2$  were determined by  $\text{NH}_3$ -TPD, as shown in Figure 9. The peaks at approximately 400 °C were attributed to Brønsted acid sites, and the peaks at approximately 600 °C were attributed to Lewis acid sites.<sup>48,49</sup>

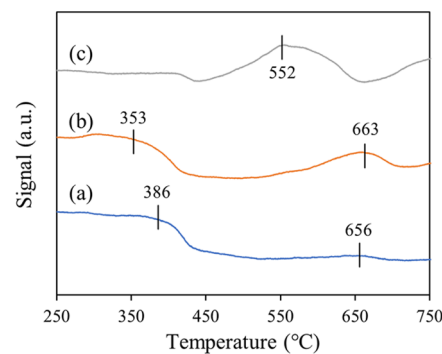


**Figure 9.**  $\text{NH}_3$ -TPD profiles of catalysts exposed to different  $\text{Cl}_2$  concentrations. Flue gas conditions: 500 ppm  $\text{NO}$ , 500 ppm  $\text{NH}_3$ , 500 ppm  $\text{SO}_2$ , and 5%  $\text{O}_2$ ; (a) 0 ppm  $\text{Cl}_2$ , (b) 25 ppm  $\text{Cl}_2$ , and (c) 30 ppm  $\text{Cl}_2$ .

As presented in Figure 9, the desorption peak of the profile under 25 ppm  $\text{Cl}_2$  (b) was larger than that of the profile under 0 ppm  $\text{Cl}_2$  (a). This means that 25 ppm  $\text{Cl}_2$  increased the number of Brønsted active sites and improved the catalytic activity. More  $\text{NH}_3$  adsorbed on the sample after exposure to 25 ppm  $\text{Cl}_2$ . However, the desorption peak at approximately 400 °C for the profile under 30 ppm  $\text{Cl}_2$  (c) was not readily apparent. The amount of Brønsted active sites decreased after

exposure to 30 ppm Cl<sub>2</sub> and the adsorption of NH<sub>3</sub> was greatly inhibited. NO<sub>x</sub> reduction efficiency also decreased when 30 ppm Cl<sub>2</sub> was added to the flue gas, as shown in Figure 2a.

Figure 10 includes the NH<sub>3</sub>-TPD profiles for the SCR catalysts after exposure to different concentrations of SO<sub>2</sub>. The

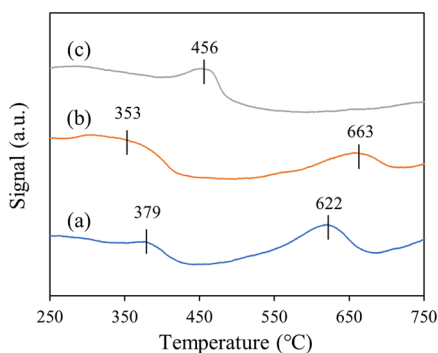


**Figure 10.** NH<sub>3</sub>-TPD profiles of catalysts exposed to different SO<sub>2</sub> concentrations. Flue gas conditions: 500 ppm NO, 500 ppm NH<sub>3</sub>, 25 ppm Cl<sub>2</sub>, and 5% O<sub>2</sub>; (a) 0 ppm SO<sub>2</sub>, (b) 500 ppm SO<sub>2</sub>, and (c) 2500 ppm SO<sub>2</sub>.

desorption peak at approximately 400 °C of the profile under 2500 ppm SO<sub>2</sub> (c) was weaker than those of the profiles under 0 ppm SO<sub>2</sub> (a) and 500 ppm SO<sub>2</sub> (b). This result shows that higher concentrations of SO<sub>2</sub> reduced the number of Brønsted active sites and suppressed the catalytic activity. The adsorption of NH<sub>3</sub> was greatly inhibited and the NO<sub>x</sub> reduction efficiency significantly decreased, as shown in Figure 4a.

When there is no Cl<sub>2</sub> in flue gas, the NH<sub>3</sub>-SCR process can be used to explain the NO<sub>x</sub> reduction by SCR catalysts.<sup>21,50–52</sup> In this study, NH<sub>3</sub> in the gas phase was first adsorbed on the catalyst surface (eq 14); a majority of the ammonia was adsorbed on Brønsted acid sites (V<sup>5+</sup>–OH) because Brønsted acid sites are active centers for SCR reactions. Then, NH<sub>3</sub> was activated by V<sup>5+</sup>=O (eq 15). The activated NH<sub>3</sub> converted NO<sub>x</sub> in the gas phase, producing N<sub>2</sub> and H<sub>2</sub>O. In the process of NO<sub>x</sub> reduction, V<sup>5+</sup>=O was transformed to V<sup>4+</sup>–OH (eq 16). Since V<sup>5+</sup> was transformed to V<sup>4+</sup>, the active sites were unable to adsorb ammonia or reduce NO<sub>x</sub>. If V<sup>4+</sup>–OH is not reoxidized to V<sup>5+</sup>=O, the SCR process may stop gradually; thus, it is necessary to regenerate the active sites. O<sub>2</sub> in the gas phase reoxidized V<sup>4+</sup>–OH to V<sup>5+</sup>=O (eq 17<sup>21,51</sup>), and then the catalysts continued to adsorb ammonia or reduce NO<sub>x</sub>. Therefore, O<sub>2</sub> is essential for regenerating the active sites. Figure 11 displays the NO<sub>x</sub> conversion by SCR catalysts under different gas conditions. When there was no O<sub>2</sub> in the flue gas, the SCR process could not operate continuously, and the NO<sub>x</sub> conversion efficiency was minimized.

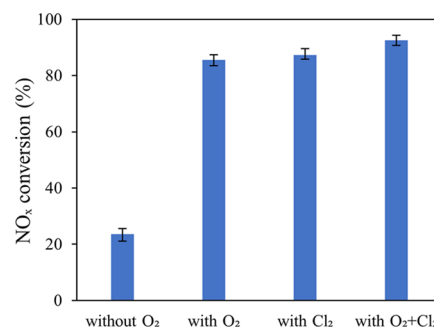
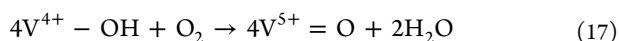
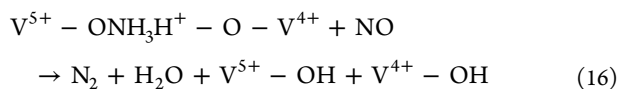
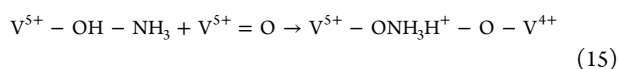
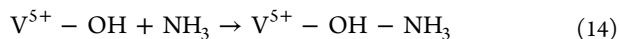
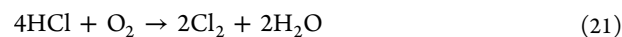
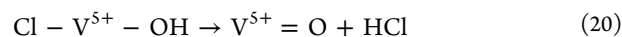
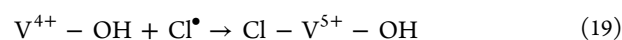


**Figure 11.** SCR catalyst NO<sub>x</sub> conversion under different gas conditions.

As Cl<sub>2</sub> was added to the flue gas, it increased the catalytic activity and oxidated V<sup>4+</sup> to V<sup>5+</sup>. The first few steps of the reaction were the same as those of the NH<sub>3</sub>-SCR reaction. NH<sub>3</sub> in the gas phase was adsorbed on the catalyst surface and activated by V<sup>5+</sup>=O, which reduced NO<sub>x</sub> in the gas phase to create N<sub>2</sub> and H<sub>2</sub>O. In the process, V<sup>5+</sup>=O was converted to V<sup>4+</sup>–OH, but Cl<sub>2</sub> could reoxidize V<sup>4+</sup>–OH to V<sup>5+</sup>=O. First, Cl<sub>2</sub> in the gas phase was converted to an active chlorine atom (Cl) on the catalyst surface (eq 18<sup>11</sup>). Then, the active chlorine atom oxidized V<sup>4+</sup>–OH to Cl–V<sup>5+</sup>–OH (eq 19<sup>11</sup>). Subsequently, Cl–V<sup>5+</sup>–OH reacted with ammonia generating V<sup>5+</sup>=O, and the intermediate substance HCl was converted to Cl<sub>2</sub> via the Deacon process (eqs 20 and 21).<sup>11,53</sup> The active sites were recreated, and they continued to adsorb ammonia or react with NO<sub>x</sub>. In this process, O<sub>2</sub> was not essential. As shown in Figure 11, when the flue gas contained Cl<sub>2</sub> but no O<sub>2</sub>, the NO<sub>x</sub> conversion efficiency was approximately 87%, which is very close to that of the O<sub>2</sub>-only condition. When the flue gas contained both Cl<sub>2</sub> and O<sub>2</sub>, the NO<sub>x</sub> conversion efficiency was approximately 93%. These results suggest that Cl<sub>2</sub> can enhance the oxidation by converting V<sup>4+</sup>–OH into V<sup>5+</sup>=O, promote the NH<sub>3</sub>-SCR process, and increase the NO<sub>x</sub> conversion efficiency.



**3.4.2. Mechanisms of Cl<sub>2</sub> Affecting Hg<sup>0</sup> Oxidation.** As presented in Figure 9, the peak at approximately 600 °C corresponded to Lewis acid sites, which are associated with Hg<sup>0</sup> oxidation. As the Cl<sub>2</sub> concentration of the samples varied from 0 to 25 ppm, the desorption peak area and signal gradually increased. This implies that the number of Lewis active sites increased, and more Hg<sup>0</sup> can adsorb on the catalyst surface and be oxidized with active chlorine on the active sites. The Hg<sup>0</sup> oxidation efficiency may have improved because the catalytic activity improved. However, the profile under 30 ppm Cl<sub>2</sub> (c) in Figure 9 had only one peak. The amount of Lewis acid sites decreased and Hg<sup>0</sup> oxidation efficiency decreased to 78%, as presented in Figure 2b.

However, as the SO<sub>2</sub> concentration of the samples varied from 0 to 2500 ppm, the desorption peak area and signal decreased, as shown in Figure 10. Higher concentrations of SO<sub>2</sub> decreased the number of Lewis active sites and suppressed the catalytic activity. The adsorption of Hg<sup>0</sup> on Lewis acid sites

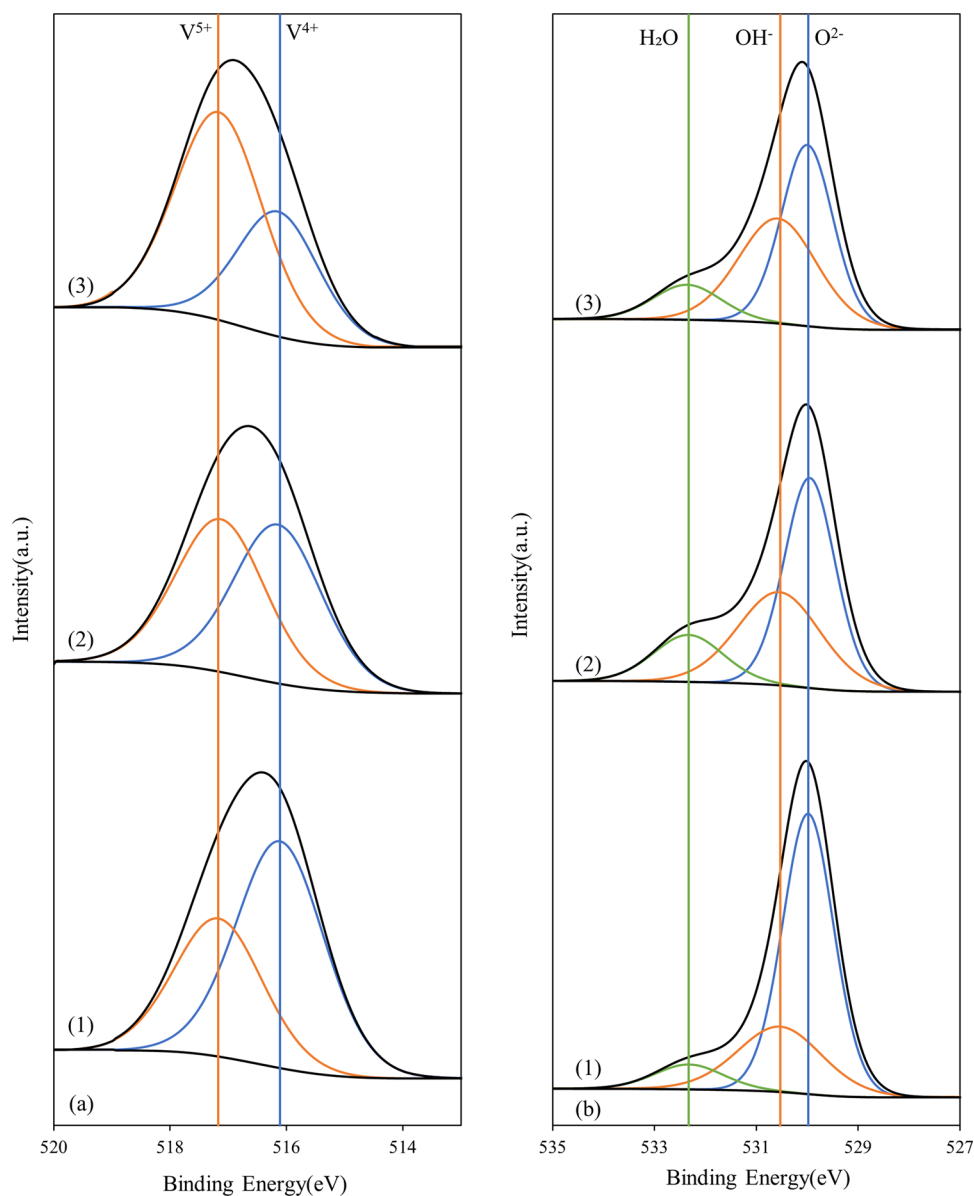
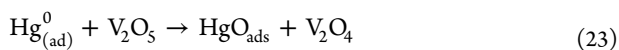


**Figure 12.** XPS spectra of the catalysts: (a) V 2p and (b) O 1s; (1) fresh SCR, (2) with 25 ppm Cl<sub>2</sub>, and (3) with 25 ppm Cl<sub>2</sub> and 500 ppm SO<sub>2</sub>.

was greatly inhibited and the Hg<sup>0</sup> oxidation efficiency decreased.

When there was no Cl<sub>2</sub> in the flue gas, Hg<sup>0</sup> oxidation by SCR catalysts followed the Mars–Maessen mechanism, and O<sub>2</sub> participated in the reaction as the oxidant.<sup>25,50</sup> First, Hg<sup>0</sup> collided on the catalyst surface and was captured by the catalyst, resulting in Hg<sup>0</sup> adsorption (eq 22). Then, Hg<sup>0</sup> reacted with lattice oxygen of vanadium pentoxide, generating adsorbed mercuric oxide (eq 23). Next, vanadium oxide was reoxidized by gas-phase oxygen and mercuric oxide desorbed from the catalyst surface (eqs 24 and 25). The mechanism of enhanced Hg<sup>0</sup> oxidation can be explained by the following reactions



When Cl<sub>2</sub> existed in the flue gas, Hg<sup>0</sup> oxidation by SCR catalysts followed the Langmuir–Hinshelwood mechanism. Gaseous Hg<sup>0</sup> was adsorbed on the active sites, and V<sup>5+</sup>–OH became V<sup>4+</sup>–O···Hg(ads) (eq 26).<sup>11,54</sup> Then, Cl<sub>2</sub> participated in the reaction transforming Hg<sup>0</sup> to Hg<sup>2+</sup>. To understand the role of vanadium sites in Cl<sub>2</sub> adsorption, the SCR catalysts were analyzed via XPS. The V 2p and O 1s peaks were used to analyze the chemical states, and the results are shown in Figure 12a,b, where (1) is for fresh SCR catalysts, (2) is for SCR catalysts with 25 ppm Cl<sub>2</sub>, and (3) is for SCR catalysts with 25 ppm Cl<sub>2</sub> and 500 ppm SO<sub>2</sub>. In Figure 12a, the binding energy value of V 2p for fresh SCR catalysts (517.2 eV) is slightly lower than the values reported in other studies for bulk vanadium (517.7 eV).<sup>55</sup> This result is consistent with the fact that vanadium well dispersed the support.<sup>11</sup> Two peaks corresponding to 517.2 and 516.1 eV were assigned to the oxidation states of V<sup>5+</sup> and V<sup>4+</sup>, respectively, via peak deconvolution. When Cl<sub>2</sub> was added into the flue gas, the

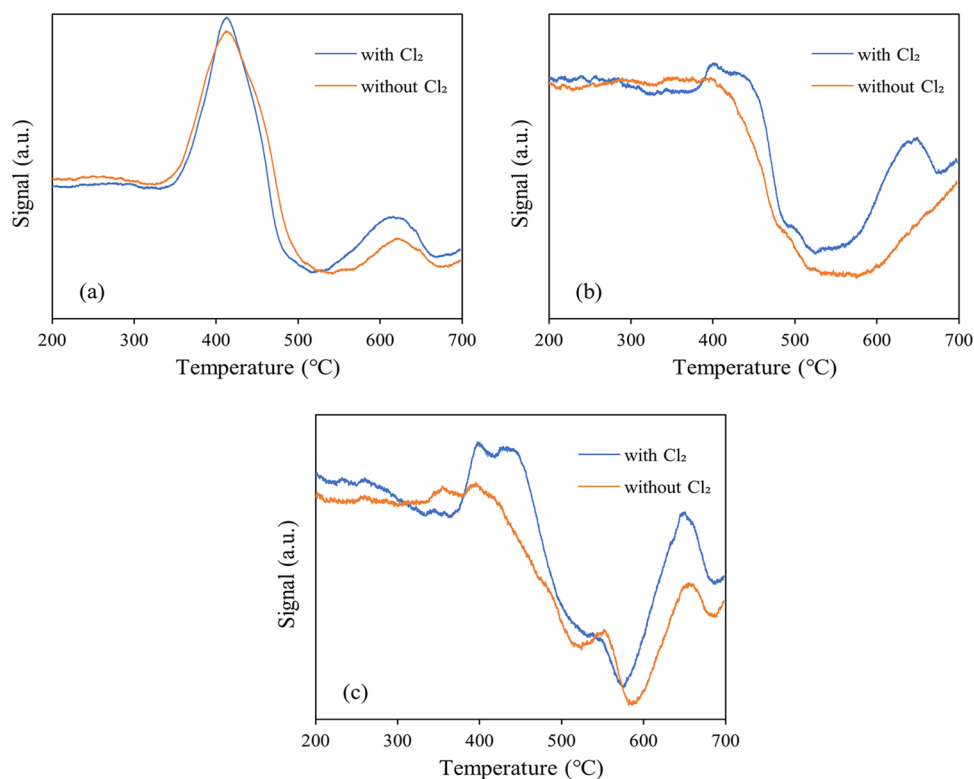
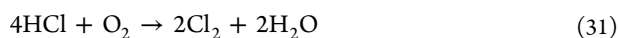
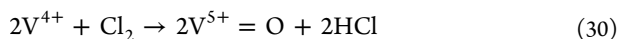
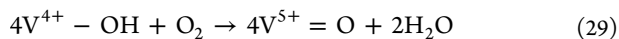
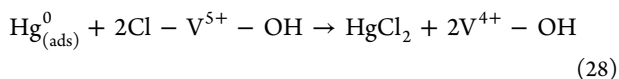
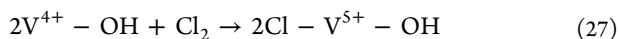
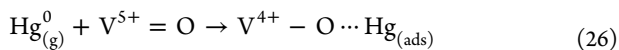


**Figure 13.**  $\text{NH}_3$ -TPD on the sulfate-poisoned catalysts with and without  $\text{Cl}_2$ : (a)  $\text{NH}_4\text{HSO}_4$ -poisoned catalysts, (b)  $\text{CaSO}_4$ -poisoned catalysts, and (c)  $\text{MgSO}_4$ -poisoned catalysts.

peaks of  $\text{V}^{5+}$  in spectra (2) and (3) were higher than that in (1). The increased peaks of  $\text{V}^{5+}$  are considered to represent the shift of the valence from  $\text{V}^{4+}$  to  $\text{V}^{5+}$  due to the electronegativity of  $\text{Cl}^-$ . The reaction is described by eq 27. Next,  $\text{Cl}-\text{V}^{5+}-\text{OH}$  reacted with adsorbed  $\text{Hg}^0$  to form  $\text{HgCl}_2$  (eq 28). Then, the reoxidation of  $\text{V}^{4+}-\text{OH}$  by  $\text{O}_2$  and  $\text{Cl}_2$  formed  $\text{V}^{5+}=\text{O}$  (eqs 29 and 30). The XPS analysis of O 1s is shown in Figure 12b. Compared with spectra (1), (2), and (3), when  $\text{Cl}_2$  was added into the flue gas, the peak of lattice oxygen ( $\text{O}^{2-}$ ) decreased, and the peak of  $\text{H}_2\text{O}$  increased. Adsorbed  $\text{Hg}^0$  was oxidized, and the sites of  $\text{V}^{4+}-\text{OH}$  species were reoxidized.<sup>11</sup> The mercury oxidation process on the vanadium-based SCR catalysts can be summarized by the following reactions



**3.4.3. Mechanism of  $\text{Cl}_2$  Affecting  $\text{NO}_x$  Reduction and  $\text{Hg}^0$  Oxidation over Sulfate-Poisoned Catalysts.** When the SCR process was operated for a long time,  $\text{NH}_4\text{HSO}_4$  was deposited on the catalyst surface,<sup>56</sup> causing pore plugging, decreasing the surface area, and inactivating the active sites.<sup>57,58</sup> According to the experimental results reported in Section 3.3.1, the addition of  $\text{Cl}_2$  into the flue gas promoted both  $\text{NO}_x$  reduction and  $\text{Hg}^0$

oxidation over  $\text{NH}_4\text{HSO}_4$  poisoned catalysts.  $\text{Cl}_2$  reoxidized  $\text{V}^{4+}$  into  $\text{V}^{5+}$ , and the growth in the number of active sites enhanced the catalytic activity. Figure 13a shows the  $\text{NH}_3$ -TPD curves of the  $\text{NH}_4\text{HSO}_4$  poisoned catalysts pretreated and not pretreated by  $\text{Cl}_2$  at temperatures ranging from 50 to 700 °C. There are two types of  $\text{NH}_3$  desorption peaks: one near 400 °C and the other near 600 °C. When the catalysts were pretreated with  $\text{Cl}_2$ , the elevation of two types of  $\text{NH}_3$  desorption peaks increased, which suggests that  $\text{Cl}_2$  increased the number of active sites and improved the catalytic activity.

Alkali metals (Ca/Mg) also affect the SCR catalysts as follows: (1) alkali metals decrease the strength and number of acid sites on  $\text{V}_2\text{O}_5\text{-WO}_3/\text{TiO}_2$  catalysts,<sup>59,60</sup> (2) they affect the surface chemisorbed oxygen and the reducibility of surface species,<sup>51,52,59,61</sup> and (3) these metals interact with tungsten species and decrease the SCR activity.<sup>59</sup>  $\text{CaSO}_4$  has a higher degree of poisoning effect than  $\text{MgSO}_4$ . However,  $\text{NO}_x$  can be reduced by  $\text{NH}_3$  over  $\text{CaSO}_4$ , thereby reducing the inhibition effect of  $\text{CaSO}_4$  on  $\text{NO}_x$  conversion efficiency.<sup>42,43</sup> When  $\text{Cl}_2$  is added to the flue gas, it increases the strength and number of acid sites. Figure 13b,c shows  $\text{NH}_3$ -TPD curves of  $\text{CaSO}_4$ - and  $\text{MgSO}_4$ -poisoned catalysts with and without  $\text{Cl}_2$  pretreatment at temperatures ranging from 50 to 700 °C. Since acid sites are the reaction center of  $\text{NO}_x$  reduction and  $\text{Hg}^0$  oxidation, the increase in the number of acid sites promotes  $\text{NO}_x$  conversion and  $\text{Hg}^0$  oxidation.  $\text{Cl}_2$  in the flue gas oxidizes  $\text{V}^{4+}-\text{OH}$  to  $\text{V}^{5+}=\text{O}$  (eq 30), making up the reduction of surface chemisorbed oxygen. Therefore,  $\text{Cl}_2$  promotes  $\text{NO}_x$  conversion and  $\text{Hg}^0$  oxidation over  $\text{CaSO}_4$ - and  $\text{MgSO}_4$ -poisoned catalysts.

## 4. CONCLUSIONS

In this study, the effects of Cl<sub>2</sub> on NO<sub>x</sub> reduction and Hg<sup>0</sup> oxidation over SCR catalysts were investigated by spraying Cl<sub>2</sub> into flue gas. The efficiency of NO<sub>x</sub> conversion and Hg<sup>0</sup> oxidation increased when the concentration of Cl<sub>2</sub> was less than 25 ppm. The optimal Cl<sub>2</sub> concentration was determined to be 25 ppm.

Then, the effect of SO<sub>2</sub> on NO<sub>x</sub> conversion and Hg<sup>0</sup> oxidation in the presence of Cl<sub>2</sub> was also investigated. Cl<sub>2</sub> decreased sulfate-toxicity inhibition on fresh SCR catalysts at low SO<sub>2</sub> concentrations (below 1500 ppm). Cl<sub>2</sub> and SO<sub>2</sub> competed for active sites on the catalysts; thus, the addition of Cl<sub>2</sub> into the flue gas decreased the number of SO<sub>2</sub>-occupied active sites compared to that when there was no Cl<sub>2</sub>. At high SO<sub>2</sub> concentrations (above 1500 ppm), SO<sub>2</sub> reacted with V<sub>2</sub>O<sub>5</sub> and NH<sub>3</sub> to generate sulfate, which covered the catalyst surface and minimized the effect of Cl<sub>2</sub>.

The effects of Cl<sub>2</sub> on different sulfur-poisoned catalysts were also studied. The number of active sites on the surface of sulfate-poisoned catalysts increased when Cl<sub>2</sub> was added. The presence of Cl<sub>2</sub> also significantly increased NO<sub>x</sub> conversion and Hg<sup>0</sup> oxidation over sulfate-poisoned catalysts.

Chlorine from cylinders was used in the experiments. In future studies, we will use industrial production methods to provide a continuous and stable chlorine supply. Wastewater from the limestone-gypsum wet flue gas desulfurization process contains a high concentration of chloride ions. Thus, in these future experiments, we will electrolyze desulfurization wastewater to generate chlorine and spray it into flue gas.

## ■ ASSOCIATED CONTENT

### SI Supporting Information

The Supporting Information is available free of charge at <https://pubs.acs.org/doi/10.1021/acsomega.2c00350>.

XRD diagram, TEM diagram, and composition analysis of commercial SCR catalyst (PDF)

## ■ AUTHOR INFORMATION

### Corresponding Author

Jiangjun Hu – School of Resource and Environmental Sciences, Wuhan University, Wuhan, Hubei 430079, P. R. China; [orcid.org/0000-0003-3916-1170](https://orcid.org/0000-0003-3916-1170); Email: [jjhu1963@outlook.com](mailto:jjhu1963@outlook.com)

### Authors

Mingxuan Ji – School of Resource and Environmental Sciences, Wuhan University, Wuhan, Hubei 430079, P. R. China; [orcid.org/0000-0002-4677-3303](https://orcid.org/0000-0002-4677-3303)

Honghu Li – Research Center for Environment and Health, Zhongnan University of Economics and Law, Wuhan, Hubei 430073, P. R. China; [orcid.org/0000-0001-8788-6577](https://orcid.org/0000-0001-8788-6577)

Kang Hu – School of Resource and Environmental Sciences, Wuhan University, Wuhan, Hubei 430079, P. R. China

Complete contact information is available at: <https://pubs.acs.org/doi/10.1021/acsomega.2c00350>

### Notes

The authors declare no competing financial interest.

## ■ ACKNOWLEDGMENTS

This work was financially supported by the program of study on electrolysis treatment of high-chlorine desulfurization

wastewater and coupled denigration and mercury oxidation technology, the program is funded by Huadian Hubei Power Generation Company Limited, Huangshi Thermal Power Branch. The authors thank the support from the Test Center of Wuhan University. They also thank the staff of Shiyanjia Lab ([www.shiyanjia.com](http://www.shiyanjia.com)) for BET, XPS, NH<sub>3</sub>-TPD, and H<sub>2</sub>-TPR analyses and language editing.

## ■ REFERENCES

- (1) Xie, Y.; Li, C.; Zhao, L.; Zhang, J.; Zeng, G.; Zhang, X.; Zhang, W.; Tao, S. Experimental study on Hg<sup>0</sup> removal from flue gas over columnar MnO<sub>x</sub>-CeO<sub>2</sub>/activated coke. *Appl. Surf. Sci.* **2015**, *333*, 59–67.
- (2) Wang, S.; Zhang, L.; Wang, L.; Wu, Q.; Wang, F.; Hao, J. A review of atmospheric mercury emissions, pollution and control in China. *Front. Environ. Sci. Eng.* **2014**, *8*, 631–649.
- (3) Zhang, H.; Zhao, J.; Fang, Y.; Huang, J.; Wang, Y. Catalytic oxidation and stabilized adsorption of elemental mercury from coal-derived fuel gas. *Energy Fuels* **2012**, *26*, 1629–1637.
- (4) Granite, E. J.; Pennline, H. W.; Senior, C. *Mercury Control: For Coal-derived Gas Streams*; John Wiley & Sons, 2015.
- (5) Hui, M.; Wu, Q.; Wang, S.; Liang, S.; Zhang, L.; Wang, F.; Lenzen, M.; Wang, Y.; Xu, L.; Lin, Z.; Yang, H.; Lin, Y.; Larsen, T.; Xu, M.; Hao, J. Mercury flows in China and global drivers. *Environ. Sci. Technol.* **2017**, *51*, 222–231.
- (6) Wang, F.; Li, G.; Wang, S.; Wu, Q.; Zhang, L. Modeling the heterogeneous oxidation of elemental mercury by chlorine in flue gas. *Fuel* **2020**, *262*, No. 116506.
- (7) Balasundaram, K.; Sharma, M. Technology for mercury removal from flue gas of coal based thermal power plants: A comprehensive review. *Crit. Rev. Environ. Sci. Technol.* **2019**, *49*, 1700–1736.
- (8) Miller, S. J.; Dunham, G. E.; Olson, E. S.; Brown, T. D. Flue gas effects on a carbon-based mercury sorbent. *Fuel Process. Technol.* **2000**, *65*–66, 343–363.
- (9) Liu, S.; Chen, J.; Cao, Y.; Yang, H.; Chen, C.; Jia, W. Distribution of mercury in the combustion products from coal-fired power plants in Guizhou, southwest China. *J. Air Waste Manage. Assoc.* **2019**, *69*, 234–245.
- (10) Zhou, Z.; Liu, X.; Hu, Y.; Xu, J.; Cao, X. E.; Liao, Z.; Xu, M. Investigation on synergistic oxidation behavior of NO and Hg<sup>0</sup> during the newly designed fast SCR process. *Fuel* **2018**, *225*, 134–139.
- (11) He, S.; Zhou, J.; Zhu, Y.; Luo, Z.; Ni, M.; Cen, K. Mercury oxidation over a vanadia based selective catalytic reduction catalyst. *Energy Fuels* **2009**, *23*, 253–259.
- (12) Ma, Y.; Mu, B.; Yuan, D.; Zhang, H.; Xu, H. Design of MnO<sub>2</sub>/CeO<sub>2</sub>-MnO<sub>2</sub> hierarchical binary oxides for elemental mercury removal from coal-fired flue gas. *J. Hazard. Mater.* **2017**, *333*, 186–193.
- (13) Zhang, Q.; Mei, J.; Sun, P.; Zhao, H.; Guo, Y.; Yang, S. Mechanism of elemental mercury oxidation over copper-based oxide catalysts: Kinetics and transient reaction studies. *Ind. Eng. Chem. Res.* **2020**, *59*, 61–70.
- (14) Wang, Z.; Liu, J.; Yang, Y.; Shen, F.; Yu, Y.; Yan, X. Elucidating the mechanism of Hg<sup>0</sup> oxidation by chlorine species over Co<sub>3</sub>O<sub>4</sub> catalyst at molecular level. *Appl. Surf. Sci.* **2020**, *513*, No. 145885.
- (15) Hall, B.; Schager, P.; Lindqvist, O. Chemical reactions of mercury in combustion flue gases. *Water, Air, Soil Pollut.* **1991**, *56*, 3–14.
- (16) Menke, R.; Wallis, G. Detection of mercury in air in the presence of chlorine and water vapor. *Am. Ind. Hyg. Assoc. J.* **1980**, *41*, 120–124.
- (17) Senior, C. L. Oxidation of mercury across selective catalytic reduction catalysts in coal-fired power plants. *J. Air Waste Manage. Assoc.* **2006**, *56*, 23–31.
- (18) Li, H.; Zhu, L.; Wang, J.; Li, L.; Shih, K. Development of nano-sulfide orbent for efficient removal of elemental mercury from coal combustion fuel gas. *Environ. Sci. Technol.* **2016**, *50*, 9551–9557.
- (19) Krishnakumar, B.; Helble, J. J. Determination of transition state theory rate constants to describe mercury oxidation in combustion

- systems mediated by Cl, Cl<sub>2</sub>, HCl and HOCl. *Fuel Process. Technol.* **2012**, *94*, 1–9.
- (20) Wu, Y.; Ali, Z.; Lu, Q.; Liu, J.; Xu, M.; Zhao, L.; Yang, Y. Effect of WO<sub>3</sub> doping on the mechanism of mercury oxidation by HCl over V<sub>2</sub>O<sub>5</sub>/TiO<sub>2</sub> (001) surface: Periodic density functional theory study. *Appl. Surf. Sci.* **2019**, *487*, 369–378.
- (21) Nakamura, K.; Muramatsu, T.; Ogawa, T.; Nakagaki, T. Kinetic model of SCR catalyst-based de-NO<sub>x</sub> reactions including surface oxidation by NO for natural gas-fired combined cycle power plants. *Mech. Eng. J.* **2020**, *7*, No. 20-00103.
- (22) Brown, M. H.; DeLong, W. B.; Auld, J. R. Corrosion by chlorine and by hydrogen chloride at high temperatures. *Ind. Eng. Chem. Res.* **1947**, *39*, 839–844.
- (23) Oh, J. M.; McNallan, M. J.; Lai, G. Y.; Rothman, M. F. High temperature corrosion of superalloys in an environment containing both oxygen and chlorine. *Metall. Mater. Trans. A.* **1986**, *17*, 1087–1094.
- (24) Sliger, R. N.; Kramlich, J. C.; Marinov, N. M. Towards the development of a chemical kinetic model for the homogeneous oxidation of mercury by chlorine species. *Fuel Process. Technol.* **2000**, *65–66*, 423–438.
- (25) Presto, A. A.; Granite, E. J. Survey of catalysts for oxidation of mercury in flue gas. *Environ. Sci. Technol.* **2006**, *40*, 5601–5609.
- (26) Kamata, H.; Ueno, Si.; Naito, T.; Yukimura, A. Mercury oxidation over the V<sub>2</sub>O<sub>5</sub>(WO<sub>3</sub>)/TiO<sub>2</sub> commercial SCR catalyst. *Ind. Eng. Chem. Res.* **2008**, *47*, 8136–8141.
- (27) Zhao, Y.; Mann, M. D.; Pavlish, J. H.; Mibeck, B. A. F.; Dunham, G. E.; Olson, E. S. Application of gold catalyst for mercury oxidation by chlorine. *Environ. Sci. Technol.* **2006**, *40*, 1603–1608.
- (28) Chi, G.; Shen, B.; Yu, R.; He, C.; Zhang, X. Simultaneous removal of NO and Hg<sup>0</sup> over Ce-Cu modified V<sub>2</sub>O<sub>5</sub>/TiO<sub>2</sub> based commercial SCR catalysts. *J. Hazard. Mater.* **2017**, *330*, 83–92.
- (29) Ma, J.; Liu, Z.; Liu, Q.; Guo, S.; Huang, Z.; Xiao, Y. SO<sub>2</sub> and NO removal from flue gas over V<sub>2</sub>O<sub>5</sub>/AC at lower temperatures-role of V<sub>2</sub>O<sub>5</sub> on SO<sub>2</sub> removal. *Fuel Process. Technol.* **2008**, *89*, 242–248.
- (30) Khodayari, R.; Ingeman Odenbrand, C. U. Regeneration of commercial SCR catalysts by washing and sulphation effect of sulphate groups on the activity. *Appl. Catal. B* **2001**, *33*, 277–291.
- (31) Saur, O.; Bensitel, M.; Saad, A. B. M.; Lavalley, J. C.; Tripp, C. P.; Morrow, B. A. The structure and stability of sulfated alumina and titania. *J. Catal.* **1986**, *99*, 104–110.
- (32) Orsenigo, C.; Lietti, L.; Tronconi, E.; Forzatti, P.; Bregani, F. Dynamic investigation of the role of the surface sulfates in NO<sub>x</sub> reduction and SO<sub>2</sub> oxidation over V<sub>2</sub>O<sub>5</sub>-WO<sub>3</sub>/TiO<sub>2</sub> catalysts. *Ind. Eng. Chem. Res.* **1998**, *37*, 2350–2359.
- (33) Frederickson, L. D.; Hausen, D. M. Infrared spectra-structure correlation study of vanadium-oxygen compounds. *Anal. Chem.* **1963**, *35*, 818–827.
- (34) Topsoe, N.-Y. Characterization of the nature of surface sites on vanadia-titania catalysts by FTIR. *J. Catal.* **1991**, *128*, 499–511.
- (35) Busca, G.; Centi, G.; Marchetti, L.; Trifiro, F. Chemical and spectroscopic study of the nature of a vanadium oxide monolayer supported on a high-surface-area TiO<sub>2</sub> anatase. *Langmuir* **1986**, *2*, 568–577.
- (36) Gao, Y.; Zhang, Z.; Wu, J.; Duan, L.; Umar, A.; Sun, L.; Guo, Z.; Wang, Q. A critical review on the heterogeneous catalytic oxidation of elemental mercury in flue gases. *Environ. Sci. Technol.* **2013**, *47*, 10813–10823.
- (37) Li, H.; Wu, C.; Li, Y.; Li, L.; Zhao, Y.; Zhang, J. Impact of SO<sub>2</sub> on elemental mercury oxidation over CeO<sub>2</sub>-TiO<sub>2</sub> catalyst. *Chem. Eng. J.* **2013**, *219*, 319–326.
- (38) Svachula, J.; Alemany, L. J.; Ferlazzo, N.; Forzatti, P.; Tronconi, E.; Bregani, F. Oxidation of sulfur dioxide to sulfur trioxide over honeycomb DeNO<sub>x</sub> catalysts. *Ind. Eng. Chem. Res.* **1993**, *32*, 826–834.
- (39) Dunn, J. P.; Koppula, P. R.; Stenger, H.; Wachs, I. E. Oxidation of sulfur dioxide to sulfur trioxide over supported vanadia catalysts. *Appl. Catal. B* **1998**, *19*, 103–117.
- (40) Shen, B.; Liu, T.; Zhao, N.; Yang, X.; Deng, L. Iron-doped Mn-Ce/TiO<sub>2</sub> catalyst for low temperature selective catalytic reduction of NO with NH<sub>3</sub>. *J. Environ. Sci.* **2010**, *22*, 1447–1454.
- (41) Qiao, S.; Chen, J.; Li, J.; Qu, Z.; Liu, P.; Yan, N.; Jia, J. Adsorption and catalytic oxidation of gaseous elemental mercury in flue gas over MnO<sub>x</sub>/Alumina. *Ind. Eng. Chem. Res.* **2009**, *48*, 3317–3322.
- (42) Yang, X.; Zhao, B.; Zhuo, Y.; Gao, Y.; Chen, C.; Xu, X. DRIFTS study of ammonia activation over CaO and sulfated CaO for NO reduction by NH<sub>3</sub>. *Environ. Sci. Technol.* **2011**, *45*, 1147–1151.
- (43) Yang, X.; Zhao, B.; Zhuo, Y.; Chen, C.; Xu, X. The investigation of SCR reaction on sulfated CaO. *Asia-Pac. J. Chem. Eng.* **2012**, *7*, 55–62.
- (44) Zhao, H.; Bennici, S.; Cai, J.; Shen, J.; Auroux, A. Effect of vanadia loading on the acidic, redox and catalytic properties of V<sub>2</sub>O<sub>5</sub>-TiO<sub>2</sub> and V<sub>2</sub>O<sub>5</sub>-TiO<sub>2</sub>/SO<sub>4</sub><sup>2-</sup> catalysts for partial oxidation of methanol. *Catal. Today* **2010**, *152*, 70–77.
- (45) Popova, G. Y.; Andrushkevich, T. V.; Semionova, E. V.; Chesalov, Y. A.; Dovlitova, L. S.; Rogov, V. A.; Parmon, V. N. Heterogeneous selective oxidation of formaldehyde to formic acid on V/Ti oxide catalysts: The role of vanadia species. *J. Mol. Catal. A: Chem.* **2008**, *283*, 146–152.
- (46) Shao, X.; Wang, H.; Yuan, M.; Yang, J.; Zhan, W.; Wang, L.; Guo, Y.; Lu, G. Thermal stability of Si-doped V<sub>2</sub>O<sub>5</sub>/WO<sub>3</sub>-TiO<sub>2</sub> for selective catalytic reduction of NO<sub>x</sub> by NH<sub>3</sub>. *Rare Met.* **2019**, *38*, 292–298.
- (47) Zhao, W.; Zhang, K.; Wu, L.; Wang, Q.; Shang, D.; Zhong, Q. Ti<sup>3+</sup> doped V<sub>2</sub>O<sub>5</sub>/TiO<sub>2</sub> catalyst for efficient selective catalytic reduction of NO<sub>x</sub> with NH<sub>3</sub>. *J. Colloid Interface Sci.* **2021**, *581*, 76–83.
- (48) Srnak, T. Z.; Dumesic, J. A.; Clausen, B. S.; Törnqvist, E.; Topsøet, N. Y. Temperature-programmed desorption/reaction and in situ spectroscopic studies of vanadia/titania for catalytic reduction of nitric oxide. *J. Catal.* **1992**, *135*, 246–262.
- (49) Ciambelli, P.; Bagnasco, G.; Lisi, L.; Turco, M.; Chiarello, G.; Musci, M.; Notaro, M.; Robba, D.; Ghetti, P. Vanadium oxide catalysts supported on laser-synthesized titania powders: Characterization and catalytic activity in the selective reduction of nitric oxide. *Appl. Catal. B* **1992**, *1*, 61–77.
- (50) Granite, E. J.; Pennline, H. W.; Hargis, R. A. Novel sorbents for mercury removal from flue gas. *Ind. Eng. Chem. Res.* **2000**, *39*, 1020–1029.
- (51) Topsoe, N. Y.; Dumesic, J. A.; Topsøe, H. Vanadia-titania catalysts for selective catalytic reduction of nitric-oxide by ammonia: II. studies of active sites and formulation of catalytic cycles. *J. Catal.* **1995**, *151*, 241–252.
- (52) Topsoe, N. Y.; Topsøe, H.; Dumesic, J. A. Vanadia/Titania catalysts for selective catalytic reduction (SCR) of nitric-oxide by ammonia: I. Combined temperature-programmed in-situ FTIR and on-line mass-spectroscopy studies. *J. Catal.* **1995**, *151*, 226–240.
- (53) Gutberlet, H.; Schluten, A.; Lienta, A. In *SCR Impacts on Mercury Emissions On Coal-fired Boilers*; EPRI SCR Workshop: Memphis, TN, 2000.
- (54) Eom, Y.; Jeon, S. H.; Ngo, T. A.; Kim, J.; Lee, T. G. Heterogeneous mercury reaction on a selective catalytic reduction (SCR) catalyst. *Catal. Lett.* **2008**, *121*, 219–225.
- (55) Madaia, G.; Elsener, M.; Koebel, M.; Raimondi, F.; Wokaun, A. Thermal stability of vanadia-tungsta-titania catalysts in the SCR process. *Appl. Catal. B* **2002**, *39*, 181–190.
- (56) Matsuda, S.; Kamo, T.; Kato, A.; Nakajima, F.; Kumura, T.; Kuroda, H. Deposition of ammonium bisulfate in the selective catalytic reduction of nitrogen oxides with ammonia. *Ind. Eng. Chem. Prod. Res. Dev.* **1982**, *21*, 48–52.
- (57) Ye, D.; Qu, R.; Zheng, C.; Cen, K.; Gao, X. Mechanistic investigation of enhanced reactivity of NH<sub>4</sub>HSO<sub>4</sub> and NO on Nb- and Sb-doped VW/Ti SCR catalysts. *Appl. Catal. A* **2018**, *549*, 310–319.
- (58) Wang, X.; Du, X.; Zhang, L.; Chen, Y.; Yang, G.; Ran, J. Promotion of NH<sub>4</sub>HSO<sub>4</sub> decomposition in NO/NO<sub>2</sub> contained atmosphere at low temperature over V<sub>2</sub>O<sub>5</sub>-WO<sub>3</sub>/TiO<sub>2</sub> catalyst for NO reduction. *Appl. Catal. A* **2018**, *559*, 112–121.

(59) Chen, L.; Li, J.; Ge, M. The poisoning effect of alkali metals doping over nano  $V_2O_5$ - $WO_3$ / $TiO_2$  catalysts on selective catalytic reduction of  $NO_x$  by  $NH_3$ . *Chem. Eng. J.* **2011**, *170*, 531–537.

(60) Kamata, H.; Takahashi, K.; Odenbrand, C. U. I. The role of  $K_2O$  in the selective reduction of  $NO$  with  $NH_3$  over a  $V_2O_5(WO_3)/TiO_2$  commercial selective catalytic reduction catalyst. *J. Mol. Catal. A: Chem.* **1999**, *139*, 189–198.

(61) Topsøe, N. Y. Mechanism of the selective catalytic reduction of nitric oxide by ammonia elucidated by in situ on-line fourier transform infrared spectroscopy. *Science* **1994**, *265*, 1217–1219.